Robust observer-based tracking control under actuator constraints for power-assisted wheelchairs

Guoxi Feng, Thierry-Marie Guerra, Lucian Busoniu, Tran Anh-Tu Nguyen, Sami Mohammad

Robust Observer-Based Tracking Control under Actuator Constraints for Power-Assisted Wheelchairs

Article *in* Control Engineering Practice · April 2021

DOI: 10.1016/j.conengprac.2020.104716

CITATIONS
6

READS
244

5 authors, including:

Thierry-Marie Guerra
Université Polytechnique Hauts-de-France
349 PUBLICATIONS **9,873** CITATIONS
SEE PROFILE

Lucian Busoniu
Universitatea Tehnica Cluj-Napoca
126 PUBLICATIONS **6,008** CITATIONS
SEE PROFILE

Anh-Tu Nguyen
Université Polytechnique Hauts-de-France
140 PUBLICATIONS **2,084** CITATIONS
SEE PROFILE

Sami Mohammad
Cyprus International University
12 PUBLICATIONS **66** CITATIONS
SEE PROFILE

Robust Observer-Based Tracking Control under Actuator Constraints for Power-Assisted Wheelchairs

Guoxi Feng[a], Thierry Marie Guerra[a,*], Lucian Busoniu[b], Anh-Tu Nguyen[a], Sami Mohammad[c]

[a] Polytechnic University Hauts-de-France UPHF, LAMIH UMR CNRS 8201, Valenciennes, France ({author}@uphf.fr)
[b] Department of Automation, Technical University of Cluj-Napoca, Romania (lucian@busoniu.net)
[c] AutoNomad Mobility Company, Valenciennes, France (sami.mohammad@autonomadmobility.com)

***Abstract* — Power-assisted wheelchairs (PWA) is an important growing market. The goal is to provide electrical assistive kits that are able to cope with a large family of disabled people and to equip a large variety of wheelchairs. This work is made in collaboration with Autonomad Mobility, a company that designs the hardware and sells Power-Assistance kits for wheelchairs. Several crucial issues arise, e.g. how to assist any Person with Reduced Mobility (PRM)? How to detect user's intentions? how to cope with the lack of system information due to excessive sensor costs. Effectively, due to the variety of wheelchairs and the different unknown PRM characteristics (mass, height, force, etc.) and pathologies, it is unrealistic to provide a solution using a precise modelling of the whole system including the wheelchair, the PRM and the ground conditions. However, proposing a safe and secure solution is obviously mandatory for this application. In particular, an on-the-market solution should be also smooth and friendly for the end-user. Estimation of the human torques is a first key point to achieve such a solution, which has been already studied in our previous works. This paper exploits these estimation results to propose a robust control law for PWA systems under saturation constraints. These constraints are unavoidable due to regulations on maximum authorized speed. From a control point of view, it resumes to an output feedback control with partially unknown references (desired speed, direction), unknown parameters (wheelchair and PRM masses, available force, ground characteristics) and input constraints. Finding an effective solution for this constrained output feedback tracking control still remains open. In this paper, we propose a two-step control design using quasi Linear Parameter Varying (q-LPV) formulation to solve this challenging control problem, i.e., first design an observer for state and unknown input estimation, and second propose a robust control scheme under parameter variations and input saturations. The control procedure is reformulated as convex optimization problems involving linear matrix inequality (LMI) constraints that can be efficiently solved with standard numerical solvers. Simulations and real-time experiments are proposed to show the effectiveness of the solution.**

***Index Terms*—Power-assisted wheelchairs, assistive control, robust torque control, Lyapunov method.**

I. INTRODUCTION

According to the 2011 world report of the World Health Organization (WHO) [1], "*About 15% of the world's population lives with some form of disability, of whom 2-4% experience significant difficulties in functioning*". Therefore, there is a high potential in research and development in this area. One of them is the general mobility of Person with Reduced Mobility (PRM) from which wheelchairs are important devices. In between, full electrical solutions [4] and purely manual wheelchairs [5], there is an important sector concerned with Power-Assisted Wheelchairs (PAW) [2]-[3]. They have a crucial role, in the sense that: electrical solutions imply a full loss of physical exercise of the PRM (detrimental for heart disease), whereas manual wheelchairs cause upper joint problems, and are not recommended for aging people or degenerative diseases. Several PAWs are available on-the-market, amongst which the motorization kits Duo [6] designed by AutoNomad Mobility, Wheeldrive [7] from Sunrise Medical and Smartdrive [8] proposed by MAX Mobility.

The manual and electrical wheelchairs are adapted to one particular PRM (generally the settings are made with the help of a physiotherapist) and her/his pathology. Moreover, for electrical wheelchair, there is no real difficulty to design the control. In the case of assistance kits, the problem is much more challenging. Effectively, the assistance strategy has to detect the intentions of the PRM (desired speed, level of assistance required) and to provide a real-time assistance safe, secure and friendly. To resume the challenge, a good assistance kit should be "wheelchair-independent and PRM-independent". None of the actual available PAW kits on-the-market are able to answer this challenge. Generally, the strategies are simplistic, i.e. current power-assisted wheelchairs on the market just assist with a power through the hand rims more or less proportional to the human measured torque, leaving much to be improved [10]-[12]. Let us review the existing strategies. Most of the proposals need to measure the human torque, generally via a push-rim sensor. It is the case for [9] where a push rim-activated power-assisted wheelchair (PAPAW) measures the human torques and interacts with the PRM via a device. As a result, the PAPAW considerably reduces the strain on the upper arm compared with manual wheelchairs. Instead of measuring human torques, an electromyogram sensor has been used in [10] associated with a disturbance observer to estimate the drivers' intention.

The assistance kits designed by the Autonomad Mobility company do not require sensors to measure the human torque, that reduces the cost of the kit in a significant way. They have been replaced with an Unknown-Input-Observer in the form of a PI-observer. It can be designed in the time domain [16] or in the angular domain corresponding to a Time-Varying Sampling [15]. These previous results show the potential of the approach for a particular user and a fixed ground condition. The challenge faced in this work is how to go from these initial results "one-user, fixed conditions" to a solution that would be the most possible "wheelchair-independent and PRM-independent". Moreover, the solution has also to face two other important

First submission to IFAC Control Engineering Practice
* Corresponding Author at UPHF guerra@uphf.fr

issues: varying ground conditions and input saturations. Remember also that the strategy has to "understand" and include the user's intention. Figure 1 summarizes the general framework. The user acts as a controller that perceives the environment to generate control signals (human torques u_h). The user gets information about the surrounding environment and her/his own state of fatigue to take a decision. The future trajectory of the PAW is derived from this information.

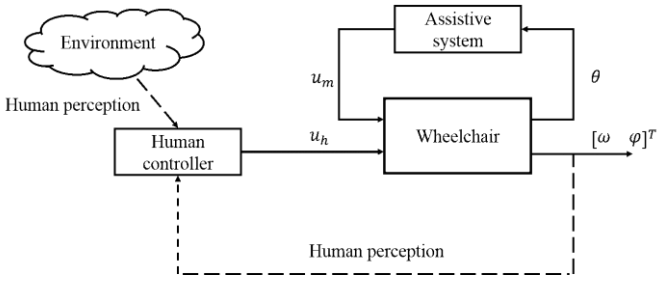

Figure 1. Human-in-the-loop power-assistance framework

To achieve these objectives, they have to be transformed into a control framework. Three main steps are necessary, presented Figure 2:

1. Robust human torque estimation $\hat{u}_h$ whatever the pushing features are; this step is achieved via a PI-Observer [15]-[16], it delivers the estimated speed and rotation of the wheelchair $\left[\hat{\omega}_k \quad \hat{\varphi}_k\right]^T$;
2. A reference trajectory generation, in order to transform the perceived intentions of the user into signals workable by the control $\left[\omega_{ref} \quad \varphi_{ref}\right]^T$;
3. A robust observer-based tracking controller design. The design has to integrate the uncertainties coming from: the human torque estimation, the measurements (environment conditions), the unknown model parameters (PRM and wheelchair masses, friction…) and the non-modelled dynamics (casters wheels). Moreover, due to regulations, the maximum speed of the wheelchair is constrained, therefore the robust control has also to take into account the actuator saturation. Finally, the overall strategy, not only must be safe and secure, but also friendly to convince the potential end-users.

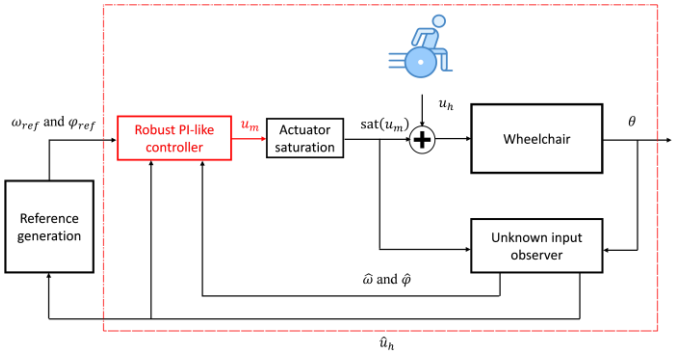

Figure 2. Assistive control loop.

Parts of the observer design and the reference generation have been respectively addressed in our previous works [15]-[16]. Mainly, the idea is not to use the amplitude of the signals estimated, due to the uncertainties they cannot be enough accurate, but to use the estimation of their frequency. This estimation is perfectly accurate to detect the user's intentions, as shown in [15]. The present work focuses on the third point mainly, which represents for robust control a class of problem without a direct solution. In order to derive a solution, the quasi Linear Parameter Varying (q-LPV) framework [17] has been used via descriptor models and a 2-step procedure. LMI constraints (Linear Matrix Inequality) problems have been derived for each step and a general proof of the global closed-loop stability is provided.

This paper is organized as follows. Section II presents the mechanical modelling of the wheelchair. Section III recalls briefly our previous works for the PI-observer and the reference generation designs. Section IV introduces the conditions to design a robust observer-based tracking controller under actuator saturations. Sections V and VI respectively provide validations of the proposed control in simulation and in real-time. Section VII gives the conclusions.

TABLE I
SYSTEM PARAMETERS

Symbol	Description	Value
ς	Wheel radius [m]	0.33
b	Distance between two wheels [m]	
d	Distance between the point a and the point c [m]	0.6
c	Centre of gravity of the wheelchair with the human	-
a	Middle point between two wheels	-
m_o	Nominal mass of wheelchair including the human [kg]	100
$\mathcal{K}_o$	Nominal viscous friction coefficient [$\mathrm{N \cdot m \cdot s}$]	5
I_a	Inertia of the wheelchair with respect to the vertical axis through the point a [$\mathrm{kg \cdot m^2}$]	16
I_0	Inertia of each driving wheel around the wheel axis [$\mathrm{kg \cdot m^2}$]	0.25
T_e	Sampling time [s]	0.05

II. MODELLING

As explained in the introduction, a precise modelling is unrealistic, therefore; the wheelchair is just considered as a two-wheeled transporter. The physical parameters of the wheelchair used for the experiments are given Table I.

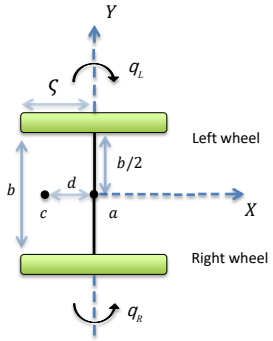

Figure 3. Simplified top view of the wheelchair

The two-wheeled PAW in Figure 3 is described by the dynamics [19]:

$$\begin{aligned}\boldsymbol{\alpha}\dot{\boldsymbol{\theta}}_R+\boldsymbol{\beta}\dot{\boldsymbol{\theta}}_L&=T_{mr}+T_{hr}-\mathcal{K}\boldsymbol{\theta}_R\\ \boldsymbol{\alpha}\dot{\boldsymbol{\theta}}_L+\boldsymbol{\beta}\dot{\boldsymbol{\theta}}_R&=T_{ml}+T_{hl}-\mathcal{K}\boldsymbol{\theta}_L\end{aligned} \tag{1}$$

where

$$\begin{aligned}\boldsymbol{\alpha}&=\frac{mr^2}{4}+\frac{\left(I_a+md^2\right)\varsigma^2}{b^2}+I_0\\ \boldsymbol{\beta}&=\frac{mr^2}{4}-\frac{\left(I_a+md^2\right)\varsigma^2}{b^2}\end{aligned} \tag{2}$$

The propulsion consists in the human torques T_{hr}, T_{hl} and the motors torques T_{mr}, T_{ml}. The left angular velocity and the right angular velocity are respectively $\boldsymbol{\theta}_L$ and $\boldsymbol{\theta}_R$. ω is the center of gravity velocity and φ the yaw velocity. They are the variables naturally and implicitly controlled by the user for her/his displacements; and directly:

$$\begin{bmatrix}\omega\\ \varphi\end{bmatrix}=\begin{bmatrix}\frac{\varsigma}{2} & \frac{\varsigma}{2}\\ \frac{\varsigma}{b} & -\frac{\varsigma}{b}\end{bmatrix}\begin{bmatrix}\boldsymbol{\theta}_R\\ \boldsymbol{\theta}_L\end{bmatrix} \tag{3}$$

Considering the sampling time $s=50ms$, imposed by the company hardware, k a sample, and $x=\begin{bmatrix}\omega & \varphi\end{bmatrix}^T$ the state vector, using Euler's approximation $\dot{x}(t)\approx\left(x_{k+1}-x_k\right)/s$, a discrete-time descriptor form is obtained. When there is no ambiguity the sample k is omitted and x^+ stands for x_{k+1}:

$$\begin{aligned}E(m)x^+&=A(m,\mathcal{K})x+Bu_h+B\text{sat}(u_m)\\ y&=Cx\end{aligned} \tag{4}$$

with $y=\begin{bmatrix}\boldsymbol{\theta}_R\\ \boldsymbol{\theta}_L\end{bmatrix}$ and $u_h=\begin{bmatrix}T_{hr}\\ T_{hl}\end{bmatrix}$, $u_m=\begin{bmatrix}T_{mr}\\ T_{ml}\end{bmatrix}$ respectively the human and motor torques. Due to regulations u_m has to be bounded with a saturation function $\text{sat}(\cdot)$ corresponding to:

$$\text{sat}\left(u_{m(\cdot)}\right)=\text{sign}\left(u_{m(\cdot)}\right)\min\left(\left|u_{m(\cdot)}\right|,u_{\max(\cdot)}\right),(\cdot)=\{l,r\} \tag{5}$$

With $u_{\max(\cdot)}$ the maximum motor torque. Considering that the motors deliver the same maximum torque for both the positive and the negative directions, (5) uses a symmetric saturation function. Both the mass m and the viscous friction coefficient $\mathcal{K}$ are uncertain, possibly time varying. They are supposed bounded in a fixed interval:

$$\underline{m}\le m\le\bar{m};\quad \underline{\mathcal{K}}\le\mathcal{K}\le\bar{\mathcal{K}} \tag{6}$$

The corresponding matrices of (4) are:

$$A(m,\mathcal{K})=\begin{bmatrix}\boldsymbol{\alpha}-T_e\mathcal{K} & \boldsymbol{\beta}\\ \boldsymbol{\beta} & \boldsymbol{\alpha}-T_e\mathcal{K}\end{bmatrix}\begin{bmatrix}\varsigma/2 & \varsigma/2\\ \varsigma/b & -\varsigma/b\end{bmatrix},\ B=T_eI_2,$$

$$E(m)=\begin{bmatrix}\boldsymbol{\alpha} & \boldsymbol{\beta}\\ \boldsymbol{\beta} & \boldsymbol{\alpha}\end{bmatrix}\begin{bmatrix}\varsigma/2 & \varsigma/2\\ \varsigma/b & -\varsigma/b\end{bmatrix},\ C=\begin{bmatrix}1/\varsigma & b/(2\varsigma)\\ 1/\varsigma & -b/(2\varsigma)\end{bmatrix}.$$

The mechanical model (4) is voluntarily simple. Extra information or modelling would require either specific knowledge, or extra sensors, or identification procedures that are not compatible with a mass production of PAW kits. The non-modelled dynamics such the casters wheels or the variations of road friction conditions do change the behavior of the wheelchair; therefore, the expectation is that (4) is enough to capture the main behavior for robust motion control design.

III. Preliminary Results

This section recalls quickly our previous results on the observer and the reference generation [15]-[16] and their extensions to the present work.

A. Observer design

Obviously, the uncertain parameters m and $\mathcal{K}$ are not measured; therefore, the state estimation is based solely on the nominal parameters m_o and $\mathcal{K}_o$ with their corresponding matrices $E_o=E(m_0)$ and $A_o=A(m_0,\mathcal{K}_0)$. A PI-observer (acting as an Unknown Input Observer) design has been proposed and validated in [16] only for the nominal case, i.e. without uncertainties. In this study, a similar observer design procedure is applied to estimate the state vector and the unknown input for the uncertain case (4). Of course, taking into account the uncertainties of (4) is of major importance to be able to deal with an observer-based control that guarantees stability and performances whatever is the mass and the ground friction according to the prescribed bounds (6). The proposed Luenberger-type PI-observer is as follows:

$$\begin{cases}E_o\hat{x}^+=A_o\hat{x}+B\text{sat}(u_m)+B\hat{u}_h+K_x\left(y-\hat{y}\right)\\ \hat{u}_h^{\ +}=\Gamma\hat{u}_h+K_{u_h}\left(y-\hat{y}\right)\\ \hat{y}=C\hat{x}\end{cases} \tag{7}$$

$\hat{x}$ is the estimation of the state vector x; as there is no torque sensor, the second row represents the PI part of the observer with $\hat{u}_h$ the estimation of the non-measured human input u_h. To capture the dynamics of the human input torques u_h, considering the motion of the input signals, Γ has been chosen as a double integrator for each torque. The observer gains K_x and K_{u_h} design follows a LMI constraints problem [16]. With the uncertain system dynamic (4) and the state observer (7), the state estimation error writes:

$$\begin{aligned}\left(E(m)-E_o\right)x^+ + E_0e_x^{\ +}&=\left(A(m,\mathcal{K})-A_o\right)x\\ &\quad+\left(A_o-K_xC\right)e_x+B\left[u_h-\hat{u}_h\right]\end{aligned} \tag{8}$$

where the estimation error is:

$$e_x=x-\hat{x} \tag{9}$$

Extra terms $\left(E(m)-E_o\right)x^+$ and $\left(A(m,\mathcal{K})-A_o\right)x$ appear into the estimation error dynamics (8) due to the uncertainties on m and $\mathcal{K}$. Considering that (8) will introduce biases in the estimation, the main question is can we still ensure a sure, safe and friendly control?

B. Reference generation

Especially, the strategy of reference generation, based on angular speed measurements and state estimation [15], has to demonstrate its capability to cope with the biases introduced by (8). This capability is mainly due to the fact that the strategy is

based on the frequency of user's propulsion, thus it is not the amplitude of the torque signals estimated $\hat{u}_h$ that is important but, the detection of its frequency. The outputs of the reference trajectory are $x_{ref} = \begin{bmatrix} \omega_{ref} & \varphi_{ref} \end{bmatrix}^T$. Note that higher (resp. lower) frequency detected corresponds to an increase (resp. a decrease) of the speed reference ω_{ref}. To turn the wheelchair, the user just brakes the wheel corresponding to the desired direction. When detected, the strategy reduces the reference center velocity ω_{ref} and generates the rotation speed reference φ_{ref} assisting the user to achieve her/his goal. To brake or stop the wheelchair (excepted an emergency stop, device available via a red stop button), the user brakes both wheels. The complete reference generation algorithm can be found in [16].

First simulation results [16] illustrate that this algorithm actively corrects the reference signal x_{ref} taking into account the changes in frequencies and direction made by users. Moreover, this important feature of the proposed strategy allows for a friendly use of the PWA solution, i.e., there is no contra-intuitive generated reference and the assistance is smooth. These performances have to be confirmed during real-time experiments.

IV. Robust Control Design

The last step is to design a robust controller, according to the mass, the unknown ground conditions and the observer biases, and also a performant controller that follows smoothly the references ω_{ref} and φ_{ref} generated under saturation constraints on the motor torques u_m, red dotted line Figure 2. The design of such a robust observer-based tracking controller under actuator saturations has no direct solution, i.e. in the sense of LMI constraints problem available.

A. Preliminaries

With the reference signal x_{ref}, the observer-based tracking error e_c is:

$$e_c = x_{ref} - \hat{x} \tag{10}$$

Knowing the estimated state $\hat{x} = x - e_x$, the tracking error (10) and the integral part e_{int} are expressed as follows:

$$\begin{aligned} e_c &= x_{ref} - x + e_x \\ e_c^{+} &= x_{ref}^{+} - x^{+} + e_x^{+} \\ e_{\text{int}}^{+} &= e_{\text{int}} + e_c \end{aligned} \tag{11}$$

We define the exogenous signal w and an extended state vector $\bar{e}$ as follows:

$$w = \begin{bmatrix} u_h \\ \hat{u}_h \\ x_{ref} \\ x_{ref}^{+} \end{bmatrix}, \quad \bar{e} = \begin{bmatrix} e_c \\ e_{\text{int}} \\ e_x \end{bmatrix} \tag{12}$$

Therefore, the uncertain system (4) and the estimation error dynamics (8) are equivalent to:

$$\bar{E}(m)\bar{e}^{+} = \bar{A}(m,\mathcal{K})\bar{e} + \bar{B}\text{sat}(u_m) + D(m,\mathcal{K})w \tag{13}$$

with the matrices:

$$\bar{E}(m) = \begin{bmatrix} -E(m) & 0 & E(m) \\ 0 & I & 0 \\ -E(m)+E_o & 0 & E(m) \end{bmatrix}, \bar{B} = \begin{bmatrix} B \\ 0 \\ 0 \end{bmatrix},$$

$$\bar{A}(m,\mathcal{K}) = \begin{bmatrix} -A(m,\mathcal{K}) & 0 & A(m,\mathcal{K}) \\ I & I & 0 \\ -A(m,\mathcal{K})+A_o & 0 & A(m,\mathcal{K})-K_xC \end{bmatrix}, \text{ and}$$

$$D(m,\mathcal{K}) = \begin{bmatrix} B & 0 & A(m,\mathcal{K}) & -E(m) \\ 0 & 0 & 0 & 0 \\ B & -B & A(m,\mathcal{K})-A_o & -E(m)+E_o \end{bmatrix}.$$

To deal with actuator saturations, we define the dead-zone function $\phi(u_m)$:

$$\phi(u_m) = u_m - \text{sat}(u_m) \tag{14}$$

Remark 1: model (13) has a descriptor form with $\bar{E}(m)$ well-defined. Therefore, using $\bar{E}^{-1}(m)$ is possible and multiplication to the left in (13) gives a perfectly equivalent classical model. Nevertheless, in view of a LMI formulation with m an unknown parameter, it is important (in the sense of attaining solutions via LMI problems) not to increase the number of vertices and to keep an input matrix $\bar{B}$ constant. The descriptor form (13) corresponds to these criteria. See the discussion and examples in section C of [24].

B. Robust Control Design

In order to achieve the tracking task, the proposed controller writes:

$$u_m = \bar{L}\bar{M}^{-1}\bar{e} + Gw \tag{15}$$

where $\bar{L}$ and $\bar{M}$ are matrices to be determined, and $G = \begin{bmatrix} 0_2 & -I_2 & G_{ref} & G_{ref^+} \end{bmatrix}$. Considering w in (12), as u_h is not directly measured, the first entry of G is 0_2; whereas the second entry of G corresponding to the unknown input estimation $\hat{u}_h$, is set to $-I_2$ [20]. The terms G_{ref} and G_{ref^+} correspond to a feedforward control part. Notice that, since the uncertain parameters m and $\mathcal{K}$ are unknown, they cannot be part of the controller (15), like for a PDC scheme [13], therefore, the control is linear.

The observer-based closed-loop system (13) together with the controller (15) writes:

$$\bar{E}(m)\bar{e}^{+} = \left(\bar{A}(m,\mathcal{K}) + \bar{B}\bar{L}\right)\bar{e} + \left(D(m,\mathcal{K}) + \bar{B}G\right)w - \bar{B}\phi(u_m) \tag{16}$$

Combined with an anti-windup strategy, the integral term of the tracking error is:

$$e_{\text{int}}^{+} = e_{\text{int}} + e_c + HS^{-T}\phi(u_m) \tag{17}$$

The closed loop system (16) with the anti-windup strategy (17) is rewritten in a quasi-LPV form as follows:

$$\sum_{i=1}^{2}\zeta_i(m)\bar{E}_i\bar{e}^{+}=\left(\sum_{i=1}^{2}\sum_{j=1}^{2}\zeta_i(m)\vartheta_j(\mathcal{K})\bar{A}_{ij}+\bar{B}\bar{L}\bar{M}^{-1}\right)\bar{e}$$
$$+\left(\sum_{i=1}^{2}\sum_{j=1}^{2}\zeta_i(m)\vartheta_j(\mathcal{K})D_{ij}+\bar{B}G\right)w+\bar{B}_a\phi(u_m) \quad (18)$$

where the closed-loop uncertain system can be represented by the convex sum of linear models whose weights will depend on the unknown parameters m and $\mathcal{K}$. The nonlinear functions $\zeta_i(m)$ and $\vartheta_j(\mathcal{K})$ share a convex sum property, i.e. $\zeta_i(m)\in[0,1]$, $\vartheta_j(\mathcal{K})\in[0,1]$, $\sum_{i=1}^{2}\zeta_i(m)=1$ and $\sum_{i=1}^{2}\sum_{j=1}^{2}\zeta_i(m)\vartheta_j(\mathcal{K})=1$ [22]. The system matrices of (18) are $i,j\in\{1,2\}$:

$$\bar{E}_i=\begin{bmatrix}-E_i & 0 & E_i\\ 0 & I & 0\\ -E_i+E_o & 0 & E_i\end{bmatrix},\bar{A}_{ij}=\begin{bmatrix}-A_{ij} & 0 & A_{ij}\\ I & I & 0\\ -A_{ij}+A_o & 0 & A_{ij}-K_xC\end{bmatrix},$$
$$\bar{B}_a=\begin{bmatrix}-B\\ HS^{-T}\\ 0\end{bmatrix},D_{ij}=\begin{bmatrix}B & 0 & A_{ij} & -E_i\\ 0 & 0 & 0 & 0\\ B & -B & A_{ij}-A_o & -E_i+E_0\end{bmatrix}.$$

with, E_i and A_{ij} defined as:

$$E_1=E(\bar{m}),E_2=E(\underline{m}),$$
$$A_{11}=A(\bar{m},\bar{\mathcal{K}}),A_{12}=A(\underline{m},\bar{\mathcal{K}}),A_{21}=A(\bar{m},\underline{\mathcal{K}}),A_{22}=A(\underline{m},\underline{\mathcal{K}}).$$

In order to add a maximum of flexibility and to enlarge the feasibility domain of solutions, we consider a parameter-dependent Lyapunov function [25], [26] of m and $\mathcal{K}$ as follows:

$$V(\bar{e})=\bar{e}^T\sum_{i=1}^{2}\sum_{j=1}^{2}\zeta_i(m)\vartheta_j(\mathcal{K})\bar{P}_{ij}\bar{e}>0 \quad (19)$$

with $i,j\in\{1,2\}$ $\bar{P}_{ij}=\bar{P}_{ij}^{T}\in\mathbb{R}^6$.

Remark 2: The friction coefficient $\mathcal{K}$ may change in time due to the time-varying ground profile and when building $V(\bar{e}^{+})$ (20), $\mathcal{K}^{+}$ will appear. However, the user's mass m does not change for a given trajectory and the parameter is therefore frozen, i.e. $m^{+}=m$.

According to Remark 2, $V(\bar{e}^{+})$ writes:

$$V(\bar{e}^{+})=\bar{e}^{+T}\sum_{i=1}^{2}\sum_{h=1}^{2}\zeta_i(m)\vartheta_h(\mathcal{K}^{+})\bar{P}_{ih}\bar{e}^{+}>0 \quad (20)$$

Remark 3: Since the output matrix C is a square invertible matrix, the state vector x is represented by $x=C^{-1}y$. Then, for the controller (15), the state estimation error e_x of the vector $\bar{e}$ is computed as follows:

$$e_x=C^{-1}y-\hat{x} \quad (21)$$

C. Control objective

For the controller design, we consider the standard assumptions: vector w and initial condition $\bar{e}(0)$ are bounded [17]. To guarantee the stability of the closed-loop (16) and the desired tracking performance in presence of actuator saturations and uncertainties, we distinguish two different cases:

O1: $w^Tw=0$: the vector $\bar{e}$ must converge asymptotically to the origin.

O2: $w^Tw\neq0$: the $\mathcal{L}_2$-norm of the vector $\bar{e}$ must be bounded for any bounded $\bar{e}(0)$ and w. Moreover, the following inequality must hold:

$$\sum_{k=0}^{\infty}\bar{e}^T\bar{C}^T\bar{C}\bar{e}<V(\bar{e}(0))+\gamma\sum_{k=0}^{\infty}w^Tw \quad (22)$$

where the matrix $\bar{C}$ is configured to achieve a good compromise between the tracking and the estimation performances.

Theorem 1. *If there exist positive definite matrices* $\bar{P}_{ij}\in\mathbb{R}^6$, *matrices* $\bar{L}\in\mathbb{R}^{2\times6}$, G_{ref}, $G_{ref^{+}}$, $H\in\mathbb{R}^{2\times2}$, $\bar{M}\in\mathbb{R}^{6\times6}$ *a positive diagonal matrix* $S\in\mathbb{R}^2$ *and a positive scalar* γ *such that for* $i,j,k\in\{1,2\}$ *:*

$$\bar{\Pi}_{ijh}^{1}+\bar{\Pi}_{ij}^{2}+\left(\bar{\Pi}_{ij}^{2}\right)^T<0 \quad (23)$$

where

$$\bar{\Pi}_{ij}^{2}=\begin{bmatrix}\epsilon\left(\bar{A}_{ij}\bar{M}+\bar{B}\bar{L}\right) & 0 & -\epsilon\bar{E}_j\bar{M} & \epsilon\bar{B}_aS^T & \epsilon\left(D_{ij}+\bar{B}G\right)\\ 0 & 0 & 0 & 0 & 0\\ \bar{A}_{ij}\bar{M}+\bar{B}\bar{L} & 0 & -\bar{E}_j\bar{M} & \bar{B}_aS^T & D_{ij}+\bar{B}G\\ 0 & 0 & 0 & 0 & 0\\ 0 & 0 & 0 & 0 & 0\end{bmatrix}$$

$$\bar{\Pi}_{ijh}^{1}=\begin{bmatrix}-\bar{M}^T\bar{P}_{ij}\bar{M} & * & 0 & * & 0\\ \bar{C}\bar{M} & -I & 0 & 0 & 0\\ 0 & 0 & \bar{M}^T\bar{P}_{ih}\bar{M} & 0 & 0\\ \bar{L} & 0 & 0 & -2S & *\\ 0 & 0 & 0 & G^T & -\gamma I\end{bmatrix}\bar{B}_aS^T=\begin{bmatrix}-BS^T\\ H\\ 0\end{bmatrix}$$

then, the observer-based controller (15) *achieves the control objective defined in* ***O1*** *and* ***O2****.*

The inequalities (23) are parameter dependent-LMIs, i.e. they reduce to LMI constraints for a given scalar ε. A numerical gridding search for $\varepsilon\in[0:0.05:10]$ is carried out in a given interval, a commonly used approach for LPV systems [27]. The complete proof of Theorem 1 is given Appendix 1.

V. Simulation Results

The robust observer-based tracking controller issued from Theorem 1 is tested first in simulation using the nominal parameters of Table I for both observer and robust control designs. The uncertain parameters variations considered are $m\in[\underline{m},\bar{m}]=[70,130]kg$ and $\mathcal{K}\in[\underline{\mathcal{K}},\bar{\mathcal{K}}]=[3,7]N.m.s$; covering most of the cases in practice. For simulation, when

$w \neq 0$ sinusoidal signals are generated to represent the user' pushing profiles. As stated Remark 2, mass is kept constant for each trial, whereas friction coefficient can be time-varying. The maximum motor torque is $u_{\max} = 30Nm$ for both electrical motors. Matrix $\bar{C}$ in (22) is set to: $\bar{C} = \begin{bmatrix} I_2 & 0_2 & 0_2 \\ 0_2 & 0_2 & I_2 \end{bmatrix}$.

Remark 4: as during maneuvers, ensuring the good turn is more important than ensuring the good speed, the yaw angle has priority on the center velocity tracking. Therefore, the weight matrix $\bar{C}$ acts similarly as the weighting matrix in a Linear-Quadratic Regulator design. It has been configured such that the observer-based control (15) ensures first the yaw velocity tracking when actuator saturations occur.

Using the design procedure [16], with nominal values $m_0 = 100kg$ and $\mathcal{K}_0 = 5N.m.s$ the state observer gains K_x and K_{u_h} (7) are:

$$K_x = \begin{bmatrix} 18.76 & -10.56 \\ -10.56 & 18.76 \end{bmatrix},\ K_{u_h} = \begin{bmatrix} 143.61 & -81.53 \\ 160.06 & -90.92 \\ -81.53 & 143.61 \\ -90.92 & 160.06 \end{bmatrix}.$$

Therefore, the robust control parameters obtained from Theorem 1 are given by:

$$\bar{L}\bar{M}^{-1} = \begin{bmatrix} 170.21 & 661.19 & 128.72 & 176.83 & -26.27 & -519.93 \\ 256.33 & -664.89 & 140.26 & -144.95 & -132.26 & 585.82 \end{bmatrix}$$

$$G = \begin{bmatrix} 0 & 0 & -1 & 0 & -10.33 & -230.3 & 17.24 & 238.26 \\ 0 & 0 & 0 & -1 & -166.86 & 808.01 & 170.55 & -818.41 \end{bmatrix},$$

$$HS^{-T} = \begin{bmatrix} -0.0063 & -0.0061 \\ -0.0014 & 0.0004 \end{bmatrix},\ \varepsilon = 0.15 \text{ and } \sqrt{\gamma} = 2716.$$

A. *Simulation results*

Numerous simulations have been conducted to validate the approach; one of them is presented, illustrating the behavior of the strategy in presence of actuator saturations and system uncertainties. The mass is set to $m = 130kg$, the viscous friction coefficient to $\mathcal{K} = 6.5N.m.s$ and the human torques are emulated via sinusoidal signals. In order to show the capabilities of the algorithm, the example presented uses trajectories to follow Figure 5 (right, yellow curves); and voluntarily asymmetric pushing, Figure 4, as well as amplitudes that will generate saturation effects. Figure 4 shows the emulated torques (in blue) and, as expected, the biases in their estimation (in red) due to the mass and friction uncertainties. Asymmetry can be seen, mainly from the difference of frequencies of the left and right signals.

Despite the biases and the asymmetry, Figure 5 (right), the signal frequencies are well estimated and the assistance operates perfectly. Left side of Figure 5 shows the motor torques generated in order to follow the desired trajectories, center velocity (top, right) and yaw velocity (bottom, right). Moreover, when a saturation occurs (red line versus blue line, left side), Figure 5 shows the strategy adopted for these moments, (indicated with arrows): a perfect tracking of the yaw velocity while smoothly downgrading the tracking of the center velocity.

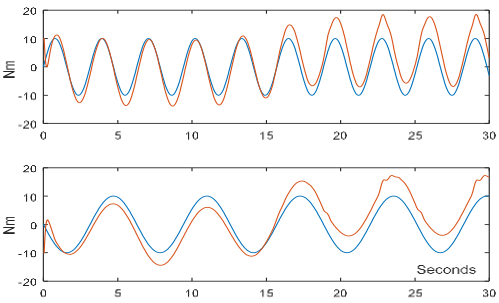

Figure 4. Emulated torques (blue) and estimated human torques (red)

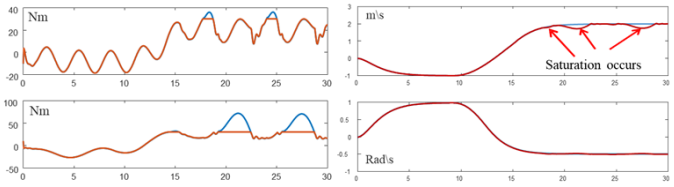

Figure 5. Assistive motor torques under actuator saturations (Left), Reference velocity and Yaw velocity of the wheelchair (Right)

Of course, the simulation part has been intensively conducted in order to fix the robustness (noise, uncertainties, saturations, different chairs and users' behaviors, pushing asymmetry…) of the whole strategy prior to real-time experiments.

VI. Experimental validation

Experimental validation is carried out with a fully equipped wheelchair from Autonomad Mobility, and in collaboration with the experts of the company. Figure 6. Two different users perform the tests using a unique controller and strategy. They are designed as: User A, who weighs 63kg (the total mass including the wheelchair is 103kg) and user B who weighs 80 kg (total mass is 120kg). When necessary different soils are available with passages from one to another.

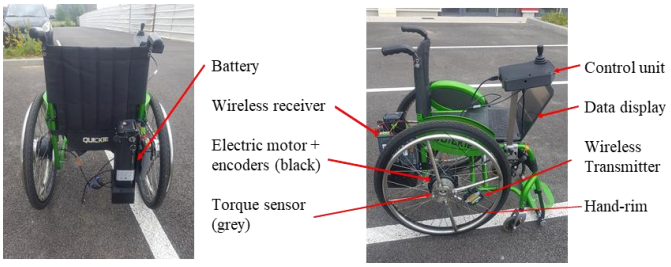

Figure 6. Wheelchair prototype and its components

The wheelchair Figure 6, is equipped with two brushless DC motors powered by a DC battery ($\sim 15km$ autonomy range). The DC motors maximum torque is around 40 Nm. The motors receive the control signals (Voltage or current) via a Texas Instruments C2000 real time micro-controller. The sensors are two incremental encoders to measure the angular velocities with pulse signals as outputs. The number of pulses is counted for a given time interval (sampling time) in order to determine the relative position between two consecutive measurements. Two torque sensors with wireless transmissions supplied by CapInstrumentation are also installed, they are only available on the prototype for the observer validation purpose.

A. *Observer validation*

This validation step does need the measurements of the human torques. Thus, the wheelchair used is an on-the-shelf wheelchair equipped with two extra torque sensors.

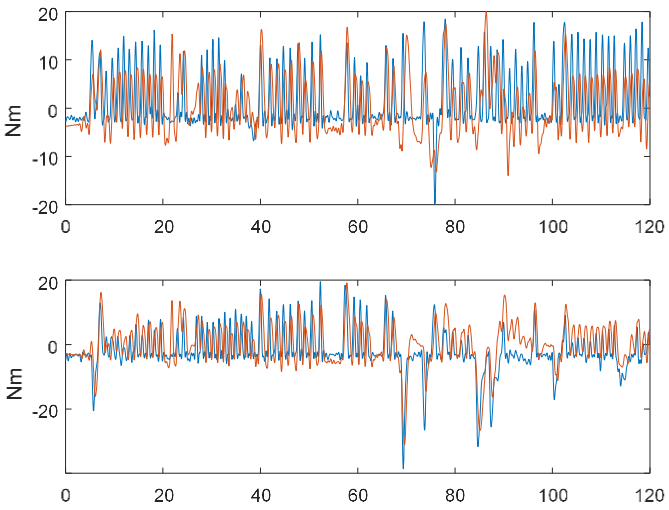

Figure 7. Left human torques estimation User A (Top) and User B (Bottom). In blue measurement, in red estimation.

The test presented, Figure 7, corresponds to a real-time 120s trial carried out by both users including different ground profiles. The only demand was for them to go straight forward. Due to ground conditions and slope variations, they have to brake sometimes one of the wheel to maintain a straight trajectory (around $t = 76s$ for User A, around $t = \{68, 72, 84, 88\}\, s$ for User B). estimation signals (in red), measured torques (in blue), top Figure 7 is user A, bottom user B. As expected, the estimated human torques do not exactly match the measured ones. The reasons are due to the uncertainties, the external conditions and moreover to the non-modelled caster wheels' dynamic. Nevertheless, and importantly, they do show that the estimated torques capture globally well the two key features of propelling for both users: pushing frequency and direction.

B. *Manual and assistance modes*

Before entering the final real-time validation, this part presents the modes (manual and assistance) and the way to switch between them. Classically, when the speed is around zero, due to the position encoders (number of teeth) there is no way to obtain a precise measurement. Naturally, this "poor" measurements cannot be directly used for control and observation as it will lead to undesired effects such as, exciting frequencies inside the electrical motors bandwidth, generating chattering effects.

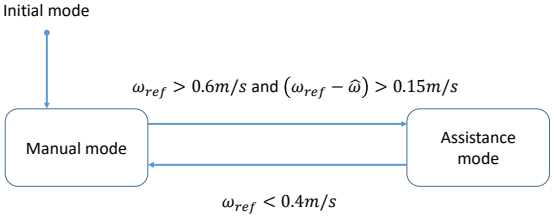

Figure 8. Manual and assistance modes

Thus, in order to ensure smooth performances, the assistance has to be disabled, when the center velocity of the wheelchair is close to zero. Thus a so-called manual mode is defined as well as an assistance mode and the conditions for switching from one to the other, Figure 8. Initially starting from manual mode, the wheelchair passes into the assistance mode when the reference center velocity achieves a given threshold, fixed at 0.6m/s. The condition $\omega_{ref} - \hat{\omega}(k) > 0.15\text{m/s}$ ensures that the estimated center velocity is lower than the reference signal at the switching moment; therefore, from manual to assistance mode, the control always provides an acceleration. The switch from assistance to manual mode occurs when the reference center velocity is below a given threshold, fixed at 0.4m/s. In order to prevent an hysteresis effect for the state machine, Figure 8 the threshold values have to be different.

C. *Assistive control validation*

The modes being defined and the observer validated, this section evaluates the full-assistive algorithm. In order to experiment the maneuverability of the wheelchair, specific predefined tasks have to be achieved by the users. For the first trial, user A has been asked to perform eight-shaped and oval trajectories (Figure 9, dotted red line) on the parking of Autonomad Mobility. This trial includes obstacle avoidance, different ground adhesions (Figure 9, clear areas) and different (reasonable) slopes. Of course, the red trajectory has not to be perfectly followed, it gives a global path to achieve. It represents for the user to perform sequentially eight turning principal actions, numbered Figure 9, right side, corresponding to: five left turns, one right turn and 2 left turns.

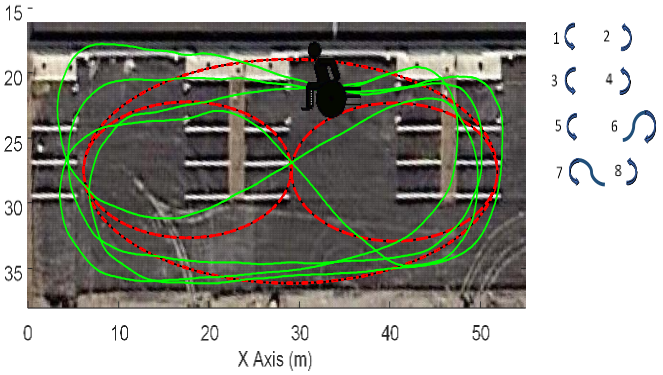

Figure 9. In red: proposed path; in green: 2 oval-shaped trajectories and one eight-shaped trajectory performed by user A under assistive control.

The human torque measured by the sensors (blue line) and the estimated human torques (red line) are given Figure 10. Again, these experimental results show that the PI-observer estimation is sufficient to produce smooth references for pushing frequency and direction, Figure 11 (red color). At the beginning, the frequency of user A is high and detected, therefore the strategy switches from the manual to the assistive mode (around $t = 10s$). Then, the eight turning actions, marked on Figure 10 and Figure 11, occur: 5 left braking (from $t = 40s$ to $t = 250s$, 5 positive right torques (Figure 10 top) corresponding to 5 negative torques, (Figure 10 bottom)), 1 right braking (the opposite around $t = 270s$) and 2 left braking. Recall that the measured torque is unavailable, therefore, not

used in the strategy. The wheelchair being equipped, for validation purpose, with torque sensors, we provide therein the comparative results.

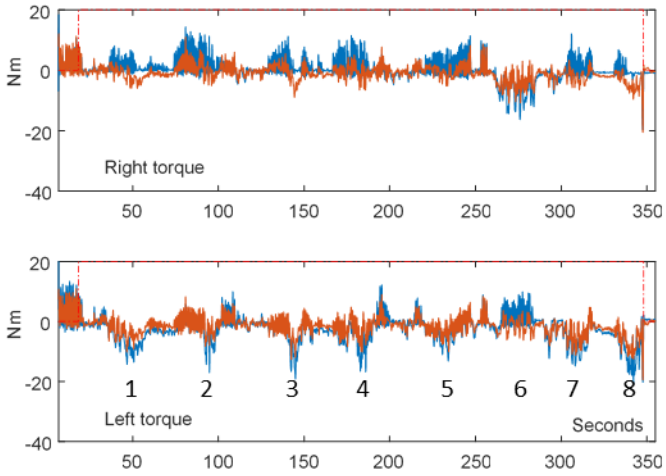

Figure 10. User A torque (blue) estimated torque (red). Mode (0 manual, 1 assistance) in dashed 0-1 line. The 8 actions are marked.

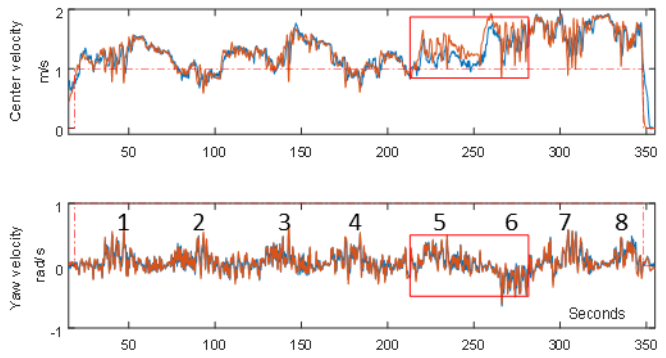

Figure 11. Center velocity (top), yaw velocity (bottom). In blue the reference generated via the strategy, in red the real outputs. Red rectangle indicates a zone where the saturation occurs. The 8 actions are marked.

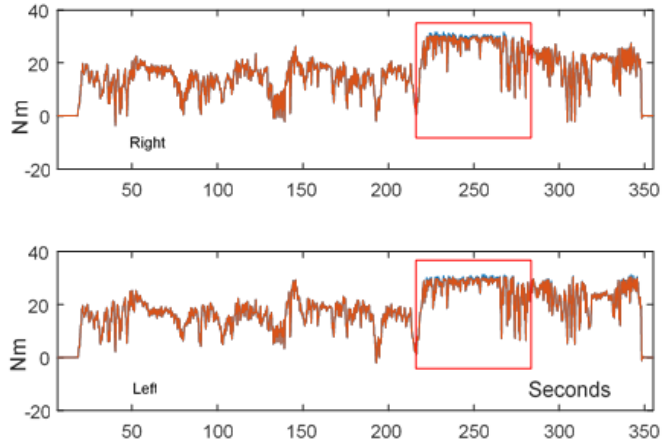

Figure 12. Motor assistive torques (User A). Red rectangle indicates a zone where the saturation occurs.

Based on the reference signals generated by the strategy Figure 11 (red color), the motor assistance torques are presented Figure 12. Between 225s and 275s (indicated by red rectangles), actuator saturations occur. Thanks to the anti-windup design (15), the overshoot of the non-saturated motor torque signal u_m (blue line of Figure 12) is perfectly controlled. Moreover, as expected, Figure 11 (red rectangles) shows an accurate tracking of the yaw velocity (bottom) while the tracking of the center velocity is smoothly downgraded (top); strategy that is one of the main objective to ensure maneuverability.

User A was able to accomplish this requested task with the help of the proposed assistive algorithm. Importantly, the strategy provided no contra-intuitive behaviors (inappropriate detection of direction, misunderstanding the "intentions") and the feedback of User A was a friendly assistance behavior.

For the second trial, user B has been asked to perform a sharp round-trip between the 2 red points, Figure 13. The figure also shows in green the trajectory of the wheelchair and the seven principal turns (right side) during the driving task, numbered sequentially.

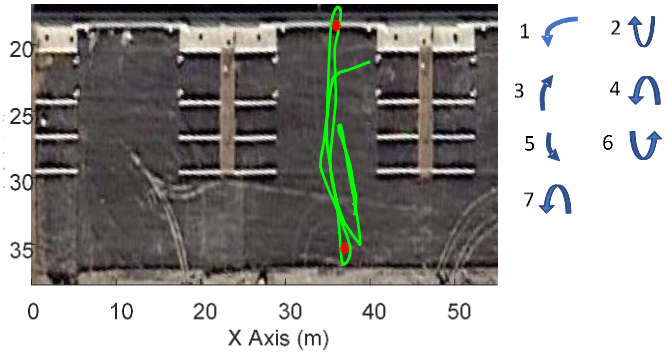

Figure 13. Round trip between two points performed by user B under the assistive control

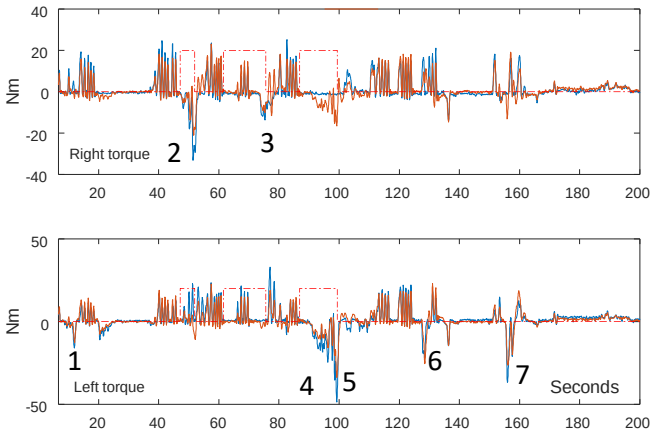

Figure 14. User B torque measured (blue) and estimated human torque (red). The dashed 0-1 line represents the mode (0 manual, 1 assistance)

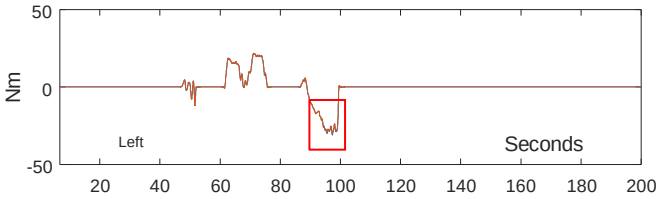

Figure 15. Assistive torque (User B). Red rectangle indicates a zone where the saturation occurs.

As previously mentioned user B is stronger, together with the fact that the roundtrip is sharp, the assistance is less activated Figure 13 red-dashed lines 0-1. It is interesting to notice that with very different conditions (user's mass, trip) and a different

behavior (human torques produced), the strategy still performs well. Figure 14 presents the human torques (blue measured, red estimated) as well as the numbering corresponding to the seven turns. Figure 15 presents one of the assistive torque, notice that a control action saturation occurs between 90s and 100s, (red rectangle) and that the assistive control acts similarly as the previous trial, i.e. the yaw velocity has priority on the tracking center velocity, Figure 16.

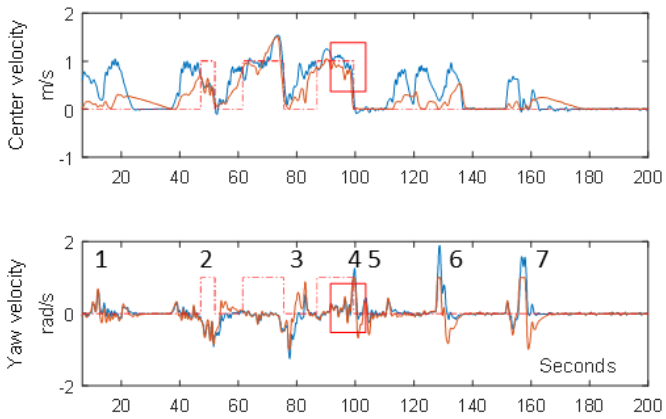

Figure 16. User B Center velocity tracking (top) and yaw velocity tracking (bottom). Red rectangle indicates a zone where the saturation occurs.

Many trials have been conducted to test the maneuverability of the proposed strategy and its robustness with respect to the mass and road conditions. The reader can refer to the link http://rocon.utcluj.ro/files/pwa_demo.mp4 for more details on some recorded trials. The results of these trials reveal that the robust output feedback tracking controller (15) satisfies the predefined objectives and the whole PWA solution provides a satisfactory performance concerning tracking control, reference generation and PI-observer based estimation.

D. Discussion and limitations

Due to heavy regulations on experimentations with disabled persons, only two users, involved in the Autonomad Mobility company, have done the trials; User B being an expert on mobility devices.

More tests have to be conducted to demonstrate the full relevance of the algorithm for an extended disabled population. Especially, the intention will be one, if not the key point to address. Robustness and PI-observer have been intensively tested in many situations to be confident on their capabilities. To exhibit problems that can occur with the intention, consider again User B experiment, Figure 13. When the user B turns abruptly (action 3, around $t = 80s$), the algorithm detects this action as a braking passing from assistance to manual mode whereas it should had kept the assistance mode. It is not an important issue in case of User B, but misinterpreting the intention can lead to deliver inadequate references and has to be avoided as possible.

This issue reaches the way are generated the references that needs to be user-adapted. Clearly, different users may perform different pushing frequency to achieve a same desired center velocity. For example, since User B is physically strong, his propelling would be high-amplitude and low-frequency; whereas medium-amplitude and medium-frequency would better represent User A. Future works are dedicated to design this user-adaptable "intention" included into the proposed model-based design, Figure 17.

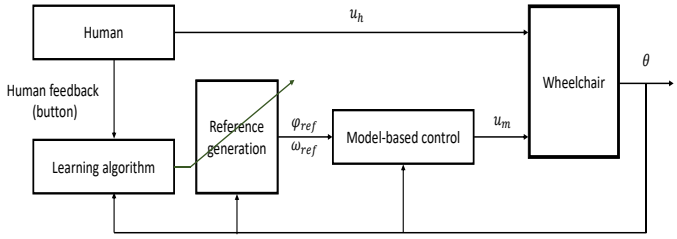

Figure 17. Control-Learning framework proposal for PAW designs

The quality of the estimated human intention depends partly on the parameter vector of the reference generation. With the help of a human feedback, a learning algorithm (based on Policy Gradient for example [28]) could produce and adapt a (near-)optimal parameter vector and generate a (near-)optimal reference signal based on the specific user. The learning approach objective would be to adapt the assistive strategies according to users' behaviors, both in the long term (for example degenerative disease) and in the "medium" term (e.g. fatigue, pain occurring during the travel).

VII. Conclusion

The goal of this work was to propose a strategy available for the PAW kits of Autonomad Mobility company with the objective of having a "wheelchair-independent and PRM-independent" kit. The strategy is decomposed in three steps: robust torque estimation to eliminate the torque sensors and reduce the price; transform the perceived intentions into signals workable by the control and propose a robust observer-based tracking controller design. Using a quasi-LPV formulation together with a descriptor description, a two-step LMI optimization problem has been derived. The first step corresponds to a PI-observer design [16]. The second step designs the robust tracking controller and ensures both the stability of the closed-loop system and the tracking performance.

For the experimental results, a step-by-step procedure allowed to validate the PI-observer (pushing frequency and direction), the reference generation algorithm and finally the complete assistive control. Based on the obtained results of this study and [18], we also propose an idea to combine the model-based approach and the model-free reinforcement learning approach.

Future works will focus on learning-control framework implementation and validation on an extended disabled population. A theoretical challenge will be to combine stability proofs and convergence issues, part of the learning, in a global framework.

APPENDIX 1

The following notations are adopted with matrices of appropriate dimension: $A_\zeta = \sum_{i=1}^{2} \zeta_i(\cdot) A_i$, for a single sum, $A_{\zeta\vartheta} = \sum_{i=1}^{2}\sum_{j=1}^{2} \zeta_i(\cdot)\vartheta_j(\cdot) A_{ij}$ for a double sum, if a different time occurs we use the subscript +, for example $A_{\vartheta\vartheta^+}$. The technical lemma 1 is useful for the proof of theorem 1.

Lemma 1. [21] Inequality of the dead-zone nonlinearity (14) $\phi(u_m) = u_m - \text{sat}(u_m)$ satisfies for any positive diagonal matrix S:

$$u_m{}^T S^{-1}\phi(u_m) + \phi^T(u_m) S^{-1} u_m - 2\phi^T(u_m) S^{-1}\phi(u_m) > 0 \tag{24}$$

***Proof of theorem 1**:* The inequality (23) can be rewritten with $\boldsymbol{J} = \begin{bmatrix} \bar{A}_{\zeta\vartheta}\bar{M} + \bar{B}\bar{L} & 0 & -\bar{E}_\zeta \bar{M} & \bar{B}_a S^T & D_{\zeta\vartheta} + \bar{B}G \end{bmatrix}$ as:

$$\bar{\Pi}^1_{\zeta\vartheta\vartheta^+} + \boldsymbol{J}^T \begin{bmatrix} \epsilon I & 0 & I & 0 & 0 \end{bmatrix} + (*) < 0 \tag{25}$$

Existence of $\bar{M}^{-1}$: from the entry $(3,3)$ of (25) it holds that:

$$\bar{M}^T \bar{P}_{\zeta\vartheta^+} \bar{M} - \bar{E}_\zeta \bar{M} - \bar{M}^T \bar{E}_\zeta^T < 0 \tag{26}$$

If $\bar{M} \in \mathbb{R}^{6\times 6}$ is singular, it exists a vector $v \in \mathbb{R}^6$, $v \neq 0$, such that $\bar{M}v = 0$, applied to (26) it contradicts the strict negativity of the expression for every $v \neq 0$, therefore, $\bar{M}$ is regular.

Using the property of congruence with the diagonal matrix $\boldsymbol{D} = diag\begin{pmatrix} \bar{M}^{-T} & I & \bar{M}^{-T} & S^{-1} & I \end{pmatrix}$, (25) is equivalent to:

$$\begin{bmatrix} -\bar{P}_{\zeta\vartheta} & * & * & * & * \\ \bar{C} & -I & * & * & * \\ 0 & 0 & \bar{P}_{\zeta\vartheta^+} & * & * \\ S^{-1}\bar{L}\bar{M}^{-1} & 0 & 0 & -2S^{-1} & * \\ 0 & 0 & 0 & G^T S^{-T} & -\gamma I \end{bmatrix} + \begin{bmatrix} \epsilon\bar{M}^{-T} \\ 0 \\ \bar{M}^{-T} \\ 0 \\ 0 \end{bmatrix} \boldsymbol{J}\boldsymbol{D}^T + \boldsymbol{D}\boldsymbol{J}^T \begin{bmatrix} \epsilon\bar{M}^{-1} & 0 & \bar{M}^{-1} & 0 & 0 \end{bmatrix} < 0 \tag{27}$$

Using the Schur's complement for the 2 first rows of (27), and defining $\tilde{\boldsymbol{J}} = \begin{bmatrix} \bar{A}_{\zeta\vartheta} + \bar{B}\bar{L}\bar{M}^{-1} & -\bar{E}_\zeta & \bar{B}_a & D_{\zeta\vartheta} + \bar{B}G \end{bmatrix}$, it holds:

$$\begin{bmatrix} -\bar{P}_{\zeta\vartheta} + \bar{C}^T\bar{C} & * & * & * \\ 0 & \bar{P}_{\zeta\vartheta^+} & * & * \\ S^{-1}\bar{L}\bar{M}^{-1} & 0 & -2S^{-1} & * \\ 0 & 0 & G^T S^{-T} & -\gamma I \end{bmatrix} + \begin{bmatrix} \epsilon\bar{M}^{-T} \\ \bar{M}^{-T} \\ 0 \\ 0 \end{bmatrix} \tilde{\boldsymbol{J}} + (*) < 0 \tag{28}$$

Now consider that the closed-loop dynamic corresponds to:

$$\bar{E}_\zeta \bar{e}^+ = \left(\bar{A}_{\zeta\vartheta} + \bar{B}\bar{L}\bar{M}^{-1}\right)\bar{e} + \left(D_{\zeta\vartheta} + \bar{B}G\right)w + \bar{B}_a\phi(u_m)$$

And equivalently to the equality constraint: $\tilde{\boldsymbol{J}} \begin{bmatrix} \bar{e} \\ \bar{e}^+ \\ \phi(u_m) \\ w \end{bmatrix} = 0$.

Therefore, via the Finsler's lemma and using the slack matrix $\begin{bmatrix} \epsilon\bar{M}^{-T} & \bar{M}^{-T} & 0 & 0 \end{bmatrix}^T$, (28) corresponds to sufficient conditions to ensure:

$$\begin{bmatrix} \bar{e} \\ \bar{e}^+ \\ \phi(u_m) \\ w \end{bmatrix}^T \begin{bmatrix} -\bar{P}_{\zeta\vartheta} + \bar{C}^T\bar{C} & * & * & * \\ 0 & \bar{P}_{\zeta\vartheta^+} & * & * \\ S^{-1}\bar{L}\bar{M}^{-1} & 0 & -2S^{-1} & * \\ 0 & 0 & G^T S^{-T} & -\gamma I \end{bmatrix} \begin{bmatrix} \bar{e} \\ \bar{e}^+ \\ \phi(u_m) \\ w \end{bmatrix} < 0 \tag{29}$$

Consider the control law $u_m = \bar{L}\bar{M}^{-1}\bar{e} + Gw$, and a parameter-dependent Lyapunov function [25], [26]:

$$V(\bar{e}) = \bar{e}^T \bar{P}_{\zeta\vartheta}\bar{e} = \bar{e}^T \sum_{i=1}^{2}\sum_{j=1}^{2} \zeta_i(m)\vartheta_j(\mathcal{K})\bar{P}_{ij}\bar{e} > 0$$

Thus, we deduce that (29) corresponds to:

$$\begin{aligned} &\Delta V(\bar{e}) + \bar{e}^T\bar{C}^T\bar{C}\bar{e} - \gamma w^T w \\ &+ u_m{}^T S^{-1}\phi(u_m) + \phi^T(u_m) S^{-1} u_m - 2\phi^T(u_m) S^{-1}\phi(u_m) < 0 \end{aligned} \tag{30}$$

The following two cases can be analyzed:

➢ *First case*: if the external signals $w = 0$, the following condition can be deduced:

$$\begin{aligned} &\Delta V(\bar{e}_c) = -\bar{e}^T\bar{C}^T\bar{C}\bar{e} - \\ &\left[u_m{}^T S^{-1}\phi(u_m) + \phi^T(u_m) S^{-1} u_m - 2\phi^T(u_m) S^{-1}\phi(u_m)\right] < 0 \end{aligned} \tag{31}$$

which means that the tracking errors converge exponentially to the origin.

➢ *Second case*: If $w \neq 0$, the inequalities in Lemma 1 and (30) imply that:

$$\Delta V(\bar{e}) + \bar{e}^T\bar{C}^T\bar{C}\bar{e} - \gamma w^T w < 0 \tag{32}$$

Under null initial conditions ($\bar{e} = 0$) and the integration of the inequality (32), we obtain:

$$\sum_{k=0}^{\infty}\left[\bar{e}^T\bar{C}^T\bar{C}\bar{e} - \gamma w^T w\right] < 0 \tag{33}$$

Then, the inequality $\sum_{k=0}^{\infty}\left(\bar{e}^T\bar{C}^T\bar{C}\bar{e}\right) < V(\bar{e}(0)) + \gamma\sum_{k=0}^{\infty} w^T w$ can be derived. Moreover, this implies the following criterion:

$$\left\|\bar{C}\bar{e}\right\|_2 < \sqrt{\gamma}\left\|w\right\|_2 \tag{34}$$

The proof of Theorem 1 is complete.

REFERENCES

[1] World Health Organization (2011). World report on disability.

[2] Seki H., Ishihara K., Tadakuma S. (2009). Novel regenerative braking control of electric power-assisted wheelchair for safety downhill road driving. *IEEE T. Industrial Electronics*, *56*(5), 1393-1400.

[3] Tashiro S., Murakami T. (2008). Step passage control of a power-assisted wheelchair for a caregiver. *IEEE T. Industrial Electronics*, *55*(4), 1715-1721.

[4] Lin J.S., Yang W.C. (2012). Wireless brain-computer interface for electric wheelchairs with EEG and eye-blinking signals. *Int Journal Innovative Computing, Information and Control*, *8*(9), 6011-6024.

[5] Van der Woude L.H., de Groot S., Janssen T.W. (2006). Manual wheelchairs: Research and innovation in rehabilitation, sports, daily life and health. *Medical engineering & physics*, *28*(9), 905-915.

[6] Mohammad S., Guerra T.M., Pudlo P. (2017). Method and device assisting with the electric propulsion of a rolling system, wheelchair kit comprising such a device and wheelchair equipped with such a device. *US Patent 10,028,871*

[7] Strautnieks M. (2001). Mid-wheel drive wheelchair. *U.S. Patent 6,196,343*

[8] MAX Mobility. PushTracker – MAX Mobility. 2016 [cited 2017 8th January]; Available from: http://www.max-mobility.com/pushtracker

[9] Cooper R.A., Corfman T.A., Fitzgerald S.G., Boninger M.L., Spaeth D.M., Ammer W., Arva J. (2002). Performance assessment of a push rim-activated power-assisted wheelchair control system. *IEEE transactions on control systems technology*, *10*(1), 121-126.

[10] Oonishi Y., Oh S., Hori Y. (2010). A new control method for power-assisted wheelchair based on the surface myoelectric signal. *IEEE T. Industrial Electronics*, *57*(9), 3191-3196.

[11] Kuo C.H., Siao J.W., Chiu K.W. (2008). Development of an intelligent power assisted wheelchair using fuzzy control systems. In *2008 IEEE Int. Conf. Systems, Man and Cybernetics*, 2578-2583

[12] Jang G., Kim J., Lee S., Choi Y. (2016). EMG-based continuous control scheme with simple classifier for electric-powered wheelchair. *IEEE T. Industrial Electronics*, *63*(6), 3695-3705.

[13] Koenig D., Mammar S. (2002). Design of proportional-integral observer for unknown input descriptor systems. *IEEE T. automatic control*, *47*(12), 2057-2062.

[14] Söffker D., Yu T.J., Müller P.C. (1995). State estimation of dynamical systems with nonlinearities by using proportional-integral observer. *International Journal of Systems Science*, *26*(9), 1571-1582.

[15] Feng G., Guerra T.M., Mohammad S., Busoniu L. (2018). Observer-Based Assistive Control Design Under Time-Varying Sampling for Power-Assisted Wheelchairs. *IFAC-PapersOnLine*, *51* (10), 151-156.

[16] Feng G., Guerra T.M., Busoniu L., Mohammad S. (2017). Unknown input observer in descriptor form via LMIs for power-assisted wheelchairs. *36th IEEE Chinese Control Conference (CCC)* 6299-6304

[17] Boyd S., Ghaoui L.E., Feron E., Balakrishnan V. (1994). Linear Matrix Inequalities in System and Control Theory. SIAM Society for Industrial and Applied Mathematics.

[18] Feng G., Busoniu L., Guerra T.M., Mohammad, S. (2019). Data-Efficient Reinforcement Learning for Energy Optimization of Power-Assisted Wheelchairs. *IEEE T. Industrial Electronics 66* (12), 9734-9744

[19] Tsai M.C., Hsueh P.W. (2012). Synchronized motion control for 2D joystick-based electric wheelchair driven by two wheel motors. *Advanced Intelligent Mechatronics (AIM), IEEE/ASME*, 702-707

[20] Chen W.H., Yang J., Guo L., Li, S. (2015). Disturbance-observer-based control and related methods – An overview. *IEEE T. Industrial Electronics*, *63* (2), 1083-1095.

[21] Mulder E.F., Tiwari P.Y., Kothare, M.V. (2009). Simultaneous linear and anti-windup controller synthesis using multiobjective convex optimization. *Automatica*, *45* (3), 805-811.

[22] Tanaka K., Wang H.O. (2001). Fuzzy control systems design and analysis: a linear matrix inequality approach. New York: John Wiley & Sons

[23] Taniguchi T., Tanaka K., Ohtake H., Wang H.O. (2001). Model construction, rule reduction, and robust compensation for generalized form of Takagi-Sugeno fuzzy systems. *IEEE T. Fuzzy Systems* 9, 525–538

[24] Estrada-Manzo V., Lendek Zs., Guerra T.M., Pudlo P. (2015). Controller design for discrete-time descriptor models: a systematic LMI approach. *IEEE T. Fuzzy Systems*, 23 (5), 1608-1621

[25] Guerra T.M., Vermeiren L. (2004). LMI-based relaxed non-quadratic stabilization conditions for nonlinear systems in the Takagi–Sugeno's form. *Automatica* 40, 823–829

[26] Ding B. (2010). Homogeneous polynomially non-quadratic stabilization of discrete-time Takagi-Sugeno systems via nonparallel distributed compensation law, *IEEE T. of Fuzzy Systems* 18 (5) 994–1000

[27] Oliveira R.C.L.F., de Oliveira M.C., Peres P.L.D. (2011). Robust state feedback LMI methods for continuous-time linear systems: Discussions, extensions and numerical comparisons, *IEEE IS Computer-Aided Control System Design*. Denver, USA, pp. 1038–1043

[28] Sutton R.S., McAllester D.A., Singh S.P., Mansour Y. (2000). Policy gradient methods for reinforcement learning with function approximation. *Advances Neural Information Processing Systems* 1057-1063